Chemically-powered swimming and diffusion in the microscopic world

Yifei Zhang and Henry Hess

Abstract | The past decade has seen intriguing reports and heated debates concerning the chemically-driven enhanced motion of objects ranging from small molecules to millimetre-size synthetic robots. These objects, in solutions in which chemical reactions were occurring, were observed to diffuse (spread non-directionally) or swim (move directionally) at rates exceeding those expected from Brownian motion alone. The debates have focused on whether observed enhancement is an experimental artefact or a real phenomenon. If the latter were true, then we would also need to explain how the chemical energy is converted into mechanical work. In this Perspective, we summarize and discuss recent observations and theories of active diffusion and swimming. Notably, the chemomechanical coupling and magnitude of diffusion enhancement are strongly size-dependent and should vanish as the size of the swimmers approaches the molecular scale. We evaluate the reliability of common techniques to measure diffusion coefficients and finish by considering the potential applications and chemical to mechanical energy conversion efficiencies of typical nanoswimmers and microswimmers.

Developing microscopic or nanoscopic machines that convert chemical energy into mechanical work or kinetic energy is an appealing but challenging task that lies at the intersection of synthetic chemistry, synthetic biology and nanotechnology[1–4]. The minuscule machines that perform work such as dragging[5], drilling[6], stirring[7] and delivering cargo[8] are also referred to as nanomotors or micromotors, depending on their size. Nature has evolved multiple sophisticated protein-based motors such as myosins, kinesins, dynein, ATP synthase, the ribosome and the flagellar motor. However, the elaborate protein folding, subtle interactions and highly ordered architectures of these motors are yet to be fully understood, which prevents the de novo fabrication of synthetic mimics with the same performance. Alternatively, scientists have tried to fabricate motors with similar functions through one of two approaches: synthesizing special molecules with rotatable chemical or mechanical bonds, or repurposing biological building blocks (protein motors, enzymes, biological assemblies or even cells) for new applications[9]. Examples of the first approach include alkene-based[10], catenane-based or rotaxane-based molecular motors[11], the discoveries of which were honoured with the 2016 Nobel Prize in Chemistry. The second approach can feature F_1-ATPase enabling rotation of actin filaments[12] or inorganic nanorods[13], kinesin propelling molecular shuttles[14,15] or sperm cells driving microrobots[16], to name but a few examples. Recently, a series of investigations suggested that common small-molecule reactants[17,18], as well as enzymes[19–21] and enzyme-coated nanostructures or microstructures[22,23], can also be considered motors because their diffusion (and, in some cases, the diffusion of the surrounding solvent molecules as well) is enhanced as a consequence of associated chemical reactions. However, the origin, magnitude and potential applications of this phenomenon have been hotly debated over the past 5 years.

Despite their structural and functional diversity, microscopic and nanoscopic motors encounter a common challenge of propelling themselves in the laminar flow regime and in the presence of strong thermal fluctuations. Purcell's scallop theorem suggests that a micromotor in laminar flow cannot gain any net displacement when undergoing reciprocal motion[24,25]. Furthermore, on the microscale, inertia becomes negligible whereas viscous forces dominate, such that a swimmer comes to a complete stop soon after propulsion ceases — within microseconds for a 1 μm particle and picoseconds for a 1 nm particle. As the size of a motor decreases, Brownian motion introduces increasingly large fluctuations in position and orientation, which can break the reciprocity of flapping motions[26] but also randomizes directed propulsion. A spherical particle in solution simultaneously undergoes translational and rotational diffusion, and its translational diffusion coefficient (D_0) and rotational diffusion coefficient (D_r) (FIG. 1a) can be described by the Einstein relations:

$$D_0 = \frac{k_B T}{6\pi\eta R} \quad (1)$$

$$D_r = \frac{k_B T}{8\pi\eta R^3} = \tau_r^{-1} \quad (2)$$

where k_B is the Boltzmann constant, T is temperature (such that $k_B T$ represents thermal energy), η is the viscosity of the solution, R is the effective hydrodynamic radius of the particle and τ_r is the characteristic rotational relaxation time. When motion is projected into two dimensions, the mean-squared displacement (MSD) $\langle \boldsymbol{x}^2 \rangle$ over a time period Δt is[27]:

$$\langle \boldsymbol{x}^2 \rangle = 4D_0\Delta t + \frac{v^2\tau_r^2}{2}\left[\frac{2\Delta t}{\tau_r} + e^{-\frac{2\Delta t}{\tau_r}} - 1\right] \quad (3)$$

When $\Delta t \ll \tau_r$, this simplifies to:

$$\langle \boldsymbol{x}^2 \rangle = 4D_0\Delta t + v^2\Delta t^2 \quad (4)$$

In the opposite case of $\Delta t \gg \tau_r$, we instead get:

$$\langle \boldsymbol{x}^2 \rangle = (4D_0 + v^2\tau_r)\Delta t = \left(4D_0 + \frac{l^2}{\tau_r}\right)\Delta t \quad (5)$$

where $l = v\tau_r$ is the average persistence length of the ballistic motion. By defining the

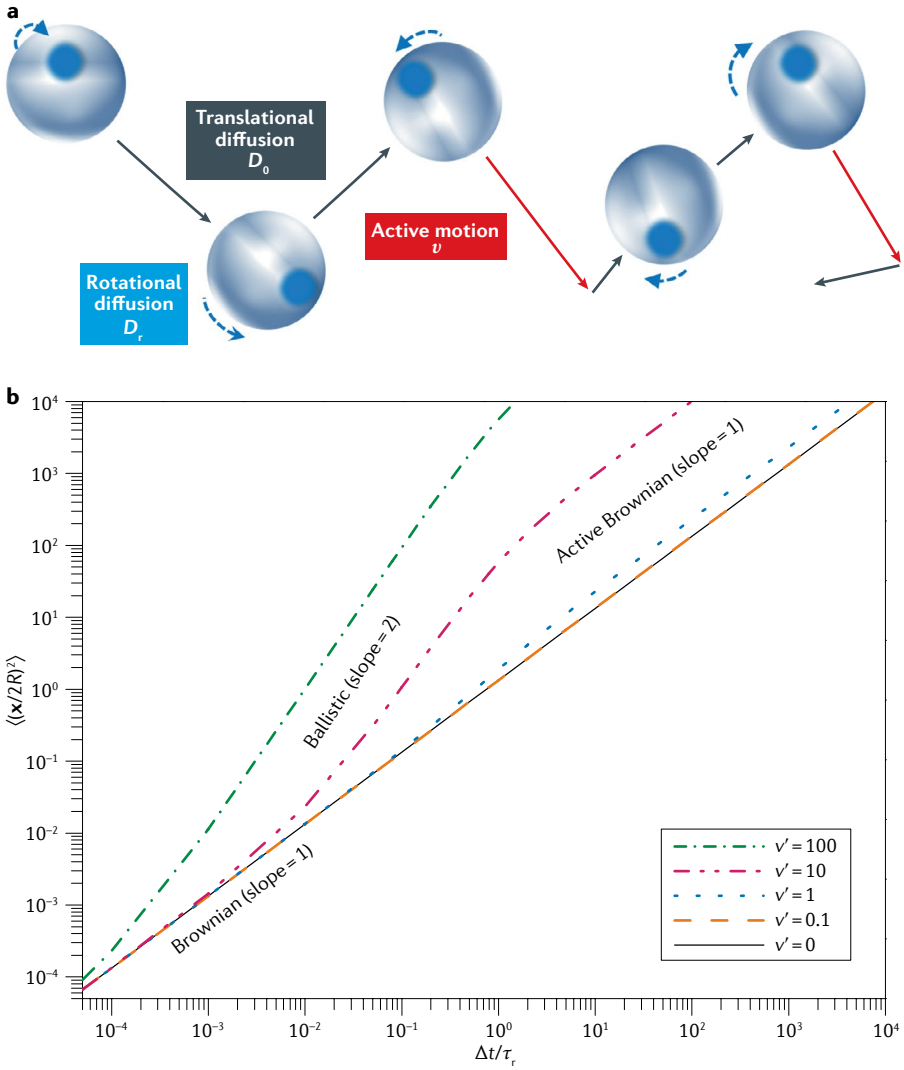

Fig. 1 | **Passive and active motion of a particle. a** | An asymmetric particle that exhibits boosted diffusion can be described by translational diffusion with diffusion coefficient D_0, rotational diffusion with diffusion coefficient D_r and concurrent active motion with velocity v. **b** | Dimensionless mean-squared displacement $\langle(\mathbf{x}/2R)^2\rangle$ (displacement scaled by the swimmer diameter $2R$) as a function of the dimensionless time $\Delta t/\tau_r$ (time scaled to the rotational relaxation time τ_r) for different dimensionless velocities $v' = v\tau_r/2R$ (velocity scaled by the quotient of diameter $2R$ to τ_r), as given by Eq. 3. R, effective hydrodynamic radius of the particle.

diffusion enhancement $\Delta D = l^2/4\tau$, this also simplifies to:

$$\langle \boldsymbol{x}^2 \rangle = (4D_0 + 4\Delta D)\Delta t \qquad (6)$$

We see that the MSD of a self-propelled particle scales linearly with Δt at the very beginning, then scales quadratically and, finally, scales linearly again as the observation time Δt greatly exceeds τ_r. Scaling the MSD by the particle diameter $2R$, Δt by τ_r and the swimming velocity v by $v^0 = 2R/\tau_r$ gives a dimensionless description of MSD[28] (FIG. 1b). For a particle to be considered a motor, it must exhibit substantial movement beyond Brownian motion, which is the case when the velocity v resulting from self-propulsion exceeds the ratio of swimmer radius and rotational relaxation time.

If we consider a particle of size $2R = 10\,\mu m$, for which $\tau_r = 10$ min in H_2O at room temperature would be typical, it is best to describe the MSD over the course of seconds because observations over this timescale will capture ballistic velocity (Eq. 4). For a much smaller particle ($2R < 10$ nm) with $\tau_r < 1\,\mu s$, directional motion is quickly randomized by particle tumbling, such that the particle exhibits apparently enhanced diffusion (Eqs. 5,6). The diffusive behaviour of a particle of size between these two regimes depends on complex factors including particle shape and the frequency and magnitude of the propulsive force, leading to a complicated time-dependent MSD. In practice, a non-linear dependence may be found as $\langle \boldsymbol{x}^2 \rangle \sim \Delta t^{\alpha}$, where $1 < \alpha < 2$. We now depict some representative chemically-driven microscopic or nanoscopic particles categorized by the above two regimes of MSD (TABLE 1).

In this Perspective, we focus on chemically-powered swimming or diffusion of microscopic objects in aqueous solution. Based on the sizes of the swimmers, we categorize recent observations into three groups: microparticles ranging in size from hundreds of nanometres to several micrometres, nanoparticles or enzymes ranging in size from a few to tens of nanometres and small molecules of subnanoscale to nanoscale dimensions. We review the origins of enhanced motion as well as the controversies associated with it, and also the occasionally observed enhanced transport of tracer particles surrounding active swimmers. The controversies often relate to the accuracy and precision with which one measures diffusion coefficients, so we discuss the reliability of common methods including particle tracking, fluorescence correlation spectroscopy (FCS), dynamic light scattering (DLS) and diffusion nuclear magnetic resonance (NMR) spectroscopy. The potential applications and the chemical to mechanical energy conversion efficiency of active swimmers are also surveyed.

Self-propelled microswimmers

Bimetallic rods can be considered the original systems for self-propelled motion on the microscale[29]. These were followed by Janus particles and enzyme-coated microbeads that are in the range of hundreds of nanometres to a few micrometres in size. Such microswimmers are most commonly actuated by electrophoresis, diffusiophoresis and bubble ejection.

Electrophoretic mechanism. Bimetallic microswimmers that directionally locomote in H_2O_2 solutions are primarily driven by electrophoresis in a self-generated electric field[30,31]. The oxidation of H_2O_2 at the anode produces protons ($H_2O_2 \rightarrow O_2 + 2H^+ + 2e^-$), whereas reduction of H_2O_2 at the cathode consumes protons ($H_2O_2 + 2H^+ + 2e^- \rightarrow 2H_2O$), establishing around the bimetallic swimmer a local electric field that points from the cathode to the anode (FIG. 2a). In turn, this self-generated electric field drives electrophoretic migration of the charged swimmer at a velocity typically in the range

of several to hundreds of micrometres per second. Such a self-electrophoretic mechanism can also propel 2 μm polypyrrole–Au rods with the two ends decorated with different haem enzymes for H_2O_2 decomposition[32], or in an inverted configuration to establish a bimetallic membrane[33]. The principal problem with this propulsion mechanism is that the H^+ current and the attendant fluid flow are confined to a space a few nanometres from the surface, such that extremely high shear is established near the no-slip surface, leading to high frictional losses.

Diffusiophoretic mechanisms. Diffusiophoresis of microparticles is caused by a concentration gradient of solutes or solvents — a chemical potential gradient[34]. The motion is driven by a diffusioosmotic slip flow at the particle–fluid interface (FIG. 2b) and the typical migration velocity is on the order of 0.1–10 μm s^{-1} (REFS[35,36]). For example, solutions with NaCl concentration gradients can see polystyrene particles diffuse at up to 1 μm s^{-1}, in proportion to the gradient of the logarithm of electrolyte concentration ($\nabla \log[\mathrm{NaCl}]$). The concentration gradients can be externally imposed or can result from salt dissolution, solute crystallization, diffusive mixing or even chemical reactions[35,36]. Among these, reaction-induced self-diffusiophoresis is of particular interest as it enables microscale/nanoscale objects to autonomously swim by generating local concentration gradients in the environment[37] (FIG. 2c).

A crude estimate of the particle motion resulting from the production of a molecule near the catalytic site (FIG. 2c) can be made by considering the osmotic pressure of the molecule on the particle while the molecule is still on one side and near the particle. If the volume in which the particle with the molecule 'on one side and near the particle' is moving is taken to be approximately equal to the volume of the particle itself, the osmotic pressure is given by $p \cong k_B T/V \approx k_B T/(2R)^3$. The resulting force $F = p\pi R^2$ on the particle over time $t \cong 4R^2/D_a = 24\pi\eta a R^2/k_B T$ is limited by the diffusive motion of the molecule away from that side. This force is opposed by the viscous drag on the particle $F = 6\pi\eta R v$, which moves a distance $vt = (\pi/2)a \cong a$. This estimate indicates that each reaction event that consumes or produces a molecule (occurring at frequency k) can lead to a displacement similar to the size of the substrate (or product) molecule, yielding a swimming velocity $v = ak$ independent of the size of the particle or the viscosity of the solution if the molecules are generated at a specific active site. For a 1 μm particle with a characteristic rotational relaxation time of 1 s, a turnover frequency of 10^3 s^{-1} could propel the particle to migrate a distance comparable with that caused by Brownian motion. Indeed, using a faster reaction or incorporating a higher spatial density of catalytic active sites aids active diffusion in experiments. However, the rapid rotational diffusion of small particles such as enzymes of size ~10 nm requires a turnover frequency exceeding 10^7 s^{-1} to manifest enhanced diffusion. This value of k exceeds the catalytic capacity of most enzymes. Immobilizing enzymes (or other catalytic

Table 1 | **Experimental observations of self-propelled particles quantified by Eq. 4 or 6**

Swimmer	Size (nm)[a]	Propelled by	D_0 (μm^2 s^{-1})	D^*_{max} (μm^2 s^{-1})[b]	v (μm s^{-1})	Ref.
Urease	14	Urea hydrolysis @ urease	31.8	40.6	–	19
Pt–Au Janus NPs	30	H_2O_2 decomposition @ Pt	10.2	12.7	–	30
Pt–Pt–Au Janus NPs	60		6.8	8.9	–	
Janus hollow mesoporous SiO_2 NPs	400	H_2O_2 decomposition @ catalase	0.75	1.30	–	23
		Urea hydrolysis @ urease	0.72	1.10	–	
		Glucose oxidation @ GOx	0.72	1.04	–	
Enzyme-coated polystyrene microparticles	790	Decomposition @ catalase	0.8	0.95	–	142
		Urea hydrolysis @ urease	0.67	0.82	–	
	2,000	H_2O_2 decomposition @ catalase	0.235	0.245	–	
HRP and cytochrome *c* modified polypyrrole–Au nanorods	260 × 1,700	O_2 oxidization of hypoxanthine @ xanthine oxidase	0.45	0.58	–	143
Pt NP-filled polymeric stomatocytes with opening	300	H_2O_2 decomposition @ Pt NPs	15[c]	–	23	144
Au–Pt nanorods	370 × 2,000	H_2O_2 decomposition @ Pt NPs	0.4	–	8	145
Polymeric stomatocytes	500	H_2O_2 decomposition @ catalase	9[c]	–	60	48
		Glucose oxidation @ catalase and GOx	9[c]	–	11	
Janus hollow mesoporous SiO_2 microparticles	2,300	Urea hydrolysis @ urease	0.2[c]	–	10	146
Bacteria attached polystyrene microbeads	10 μm	*Serratia marcescens* metabolism	0.04[c]	–	1.81 (non-chemotactic)	147
				–	3.29 (chemotactic)	
Natural tissue of radish	1 mm × 7 mm	Catalase and peroxidase	–	–	5	148
		Modified with external catalase	–	–	20	
Conductive C fibres	7 μm × 0.5–1 cm	O_2 oxidization of glucose @ GOx and BOD	–	–	10^4 [d]	149

BOD, bilirubin oxidase; D_0, translational diffusion coefficient; GOx, glucose oxidase; HRP, horseradish peroxidase; NP, nanoparticle; *v*, velocity. [a]Spherical particles are described by their diameters and cylindrical particles by their diameter × length. Units are nanometres unless otherwise stated. [b]D^*_{max} is the maximum diffusion coefficient observed in the corresponding references. [c]Estimated based on swimmer size. [d]At the air–H_2O interface.

components) on microparticles is a proven strategy to fabricate self-propelled micromotors because it maximizes the turnover events by employing multiple 'engines'. At the same time, having a larger, micrometre-scale 'body' leads to the desired reasonably slow rotational diffusion. As has been demonstrated experimentally, only micromotors coated with fast enzymes, such as urease and acetylcholinesterase, show diffusion enhancement[38]. Having an asymmetrical distribution of active sites on a particle is also crucial to the effectiveness of this type of micromotor[39].

Bubble propulsion. Pioneering work has described how a millimetre-size polydimethylsiloxane 'boat' performs Pt-catalysed H_2O_2 decomposition to power its swimming at a liquid–air interface[40]. Later efforts include the construction of differently shaped motors (such as rods[41], tubules[42], Janus spheres[43] and hollow particles with openings[44]) and the exploitation of new propellants (such as bimetallic alloys, catalytic metal or metal oxide particles[45], metals that evolve H_2 from H_2O or acids[46], enzymes[47] or enzyme cascades[48,49]). We classify diverse micromotors into three categories based on the fuels that they consume: H_2O_2, metals and biomolecules such as glucose. H_2O_2-fuelled motors have been extensively studied and a relatively high concentration of H_2O_2 is required to sustain a reasonable swimming speed, which severely limits their biomedical applications. The first metal-fuelled motors were Janus microspheres partially coated with an Al–Ga alloy that reacts with H_2O and produces H_2 (REF.[46]). Later came Zn-based and Mg-based counterparts that could self-propel in the stomach or gastrointestinal tract, greatly advancing their application in drug delivery[8,50,51]. These motors have a limited supply of metal on board and do not need to harvest fuel from their surroundings. Lastly, biomolecule-fuelled reactions can enable micromotors to operate by harvesting fuel molecules (such as glucose, ATP and O_2) under physiological conditions. For example, bowl-shaped nanoreactors with compartmentalized enzyme cascades consume glucose and phosphoenolpyruvate and exhibit enhanced motion as a result[48,49]. Using enzyme cascade reactions greatly expands the scope of fuel molecules and will help in vivo applications of synthetic micromotors. Modifying the surface of a swimmer to allow for bubbles to form and detach faster can effectively increase the propulsion speed[52], which typically is in the range 1–1,000 μm s^{-1} (REF.[53]). This is entirely plausible based on a back-of-the-envelope calculation of swimming speed. Assuming, as is often observed[42,44], that bubbles are roughly equal in radius to the swimmer and each bubble propels the swimmer by $2R$, the swimming velocity v is given by $v = kk_BT/2R^2p$, where k is the rate of production of gas molecules and p is the pressure in the bubble (approximately equal to atmospheric pressure). Note that the displacement per gas molecule produced $k_BT/2R^2p$ multiplied by the Stokes drag of the particle $6\pi\eta R$ yields the work done per reaction, which can reach a substantial fraction of the chemical energy consumed for particles smaller than 1 μm. Unfortunately, bubble formation competes against dissolution of gas molecules into the surrounding solvent, a process that prevents the formation of bubbles at the slow reaction rates typical for smaller swimmers.

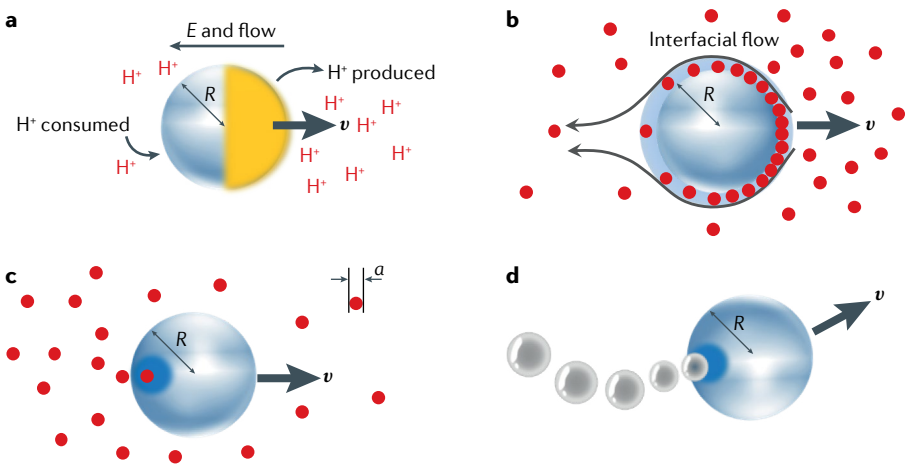

Fig. 2 | **Self-propulsion mechanisms of enhanced diffusion. a** | Electrophoresis of a Janus particle driven by a self-produced [H^+] gradient, for example from concomitant reduction and oxidation of H_2O_2 at the blue and yellow hemispheres, respectively. **b** | Diffusiophoresis of a non-reactive particle in response to an imposed concentration gradient of solute molecules (red). **c** | Diffusiophoresis of a catalytic particle that produces an anisotropic distribution of products. **d** | Bubbles can propel a particle in the opposite direction to bubble travel. R, effective hydrodynamic radius of the particle; v, velocity.

Enhanced diffusion of enzymes and nanoparticles

If we move from microscale particles to smaller swimmers ($2R < 100$ nm), we now find that ballistic motion is quickly randomized by rotation, resulting in Brownian-type diffusion with greater diffusion coefficients (FIG. 1b). Various enzymes and nanoparticles have been reported to diffuse faster when a reaction is occurring but the underlying mechanisms, and even the observations themselves, are still under discussion. In this section, we consider catalysis-induced enhanced diffusion as well as the non-catalytic case.

Catalysis-induced diffusion. Proteins and nanoparticles from several to tens of nanometres in size play a crucial role in translating molecular events into macroscopic functionalities. For instance, highly evolved protein motors such as kinesin and ATP synthase efficiently perform mechanical work by coupling a catalytic cycle to a cycle of mechanical motion. It is natural to ask whether other enzymes could also use a portion of free energy from their catalytic reactions to power their locomotion (FIG. 3a). Measurements by Sen's group first indicated that the diffusion coefficient of urease increased by 16–28% in the presence of its substrate urea[19]. Such an increase seemed to follow a Michaelis–Menten-like dependence on the urea concentration. Following this example, other enzymes, including catalase[21], alkaline phosphatase[21], acetylcholinesterase[54], hexokinase[55] and even the endothermic aldolase[56], were examined by different groups and shown to have similar magnitudes of diffusion enhancement. These results quickly sparked hot debates, which initially focused on the origin of enhancement but ended up with mounting contradictory claims that are difficult to reconcile[54,56–62]. Theoretical calculations suggested that the effect of diffusion enhancement should be much smaller than had been measured using FCS. Indeed, to increase the diffusion coefficient

by 30%, the stroke size of an enzyme would have to be an order of magnitude larger than its hydrodynamic radius[63]. Moreover, the energy released from common enzymatic reactions is insufficient to sustain the diffusion enhancement[64]. Although conformational changes of an enzyme can decrease its hydrodynamic radius and lead to higher diffusivity without the need for additional energy consumption, the corresponding shrinkage is typically less than 5%, which is far from what is necessary for the apparent 30% enhancement[65].

Aside from FCS measurements, there are other, independent methods to test the effect of enhanced diffusion. For example, DLS has been used to determine the diffusion coefficient of an aldolase in the presence and absence of its fructose-1,6-bisphosphate substrate[66], a measurement that was also carried out using pulsed-field gradient NMR spectroscopy[67]. Both experiments did not indicate any diffusion enhancement for aldolase. By using anti-Brownian electrokinetic trap-based single-molecule diffusometry, even alkaline phosphatase, a fast enzyme with a high typical turnover frequency of $10^4\,s^{-1}$, showed no diffusion enhancement during catalysis[68]. A comprehensive summary and discussion of the inconsistent experimental observations can be found in a recent critical review[69].

A very recent investigation reiterated the claims regarding enhanced diffusion of seven enzymes that catalyse exergonic reactions, including urease, phosphoglucoisomerase, acetylcholinesterase, hexokinase and others[70]. The reported magnitude of enhanced diffusion has a clear linear dependence on the Gibbs free energy release (ΔG) rate rather than the enthalpy change (ΔH), allowing for enhanced diffusion of enzymes such as aldolase, which catalyses an endothermic ($\Delta H > 0$) but exergonic ($\Delta G < 0$) reaction. However, the detailed mechanism of how free energy changes drive enhanced diffusion remains unknown. We must not forget that when the enzymatic reaction approaches equilibrium ($\Delta G = 0$), the enzymes are still catalysing the forward and reverse reactions at equal rates. As Astumian has repeatedly pointed out[71–73], individual enzymes have no awareness of the bulk reaction conditions, so for the enhanced diffusion to cease at equilibrium, the reverse reaction would have to precisely undo the movement of the forward reaction. The diffusive rotation between the reaction events makes this difficult to conceive.

The above contradictions implied the necessity to investigate the accuracy of fluorescence correlation measurements. A detailed experimental study described the potential sources of artefacts in FCS measurements of protein diffusion, revealing that the apparent diffusion of alkaline phosphatase originated from fluorescence quenching[74]. Another group found that the FCS artefacts were mainly from 4-nitrophenylphosphate-induced fluorescence quenching and blinking[68]. Dissociation of multimeric enzymes during catalysis has also been considered a possible origin of the observed enhanced diffusion of enzymes[65,74]. This hypothesis has been tested with urease, hexokinase, acetylcholinesterase and aldolase using four independent measurements: static light scattering, size-exclusion chromatography, DLS and FCS[75]. Each enzyme dissociates into its subunits at substrate concentration regimes exceeding the enzyme's Michaelis–Menten constant K_m. Although it is intuitive that substrate binding and the associated conformational changes can destabilize a multimeric enzyme complex, it is unclear why this would occur only with substrate concentration $> K_m$. In comparison, molecular tracking with total internal reflection fluorescence microscopy showed the presence of multiple oligomeric states of urease as well as a 3-fold increase in its diffusion coefficient, although the authors concluded that the enhanced diffusion was not caused by enzyme dissociation[76]. This molecular tracking was conducted in a highly viscous solution (0.6% 88-kDa methylcellulose was added to slow diffusion and aid visualization) and it is unclear whether the conclusion can be generalized to common aqueous systems. Most importantly, the reliability of MSD analysis itself has recently been questioned[77], which we will return to in a later section.

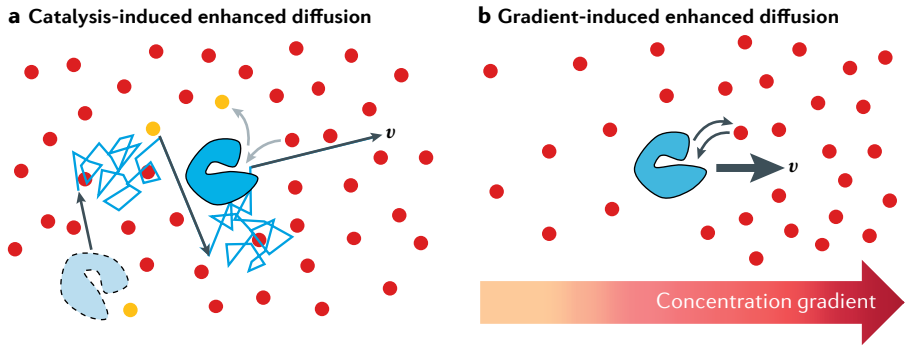

Fig. 3 | **Enhanced diffusion of a particle under catalytic and non-catalytic conditions.** **a** | Catalysis-induced enhanced diffusion was thought to originate from ballistic leaps driven by chemical reactions, independent of a concentration gradient of solutes. **b** | Enhanced diffusion occurs in the presence of a concentration gradient of substrates or products, relying on interactions between swimmers and solutes rather than any reactions directly. *v*, velocity.

The present principles are not unique to enzymes. Nanoparticles that are tens of nanometres in diameter are subject to the same limits in sustaining the accelerated diffusion by chemical reactions unless the nanoparticles undergo diffusiophoresis or chemotaxis in a concentration gradient[30].

Chemotaxis. Similar to microparticles, nanoparticles and macromolecules (especially enzymes) also exhibit migration in a solute or solvent concentration gradient. This is called chemotaxis when migration is towards regions of higher solute concentration, and antichemotaxis[54] when migration is towards lower solute concentration (FIG. 3b). This phenomenon is generally observed in microfluidic devices and has been proposed as a principle for separation[78]. The mechanism responsible for this behaviour has been proposed to be diffusiophoresis arising from non-specific interactions between particles and solutes[79] or specific active site–substrate binding[55,80]. The chemotactic migration of enzymes, which is regulated by the local substrate concentration and the substrate–enzyme binding constant, has been used to rationalize the formation of metabolons from glycolytic enzymes — enzyme complexes in which the product of one enzyme is passed to the next enyzme[55,81].

Diffusion of small molecules in reactions

The size of a small molecule is comparable with that of the surrounding solvent molecules, so any self-propelled motion of the molecule in question is rapidly randomized by the frequent collisions with solvent ($D_r = 10^9$–$10^{12}\,s^{-1}$)[82]. In the absence of chemical reactions, the translational diffusion coefficient is given by the classic

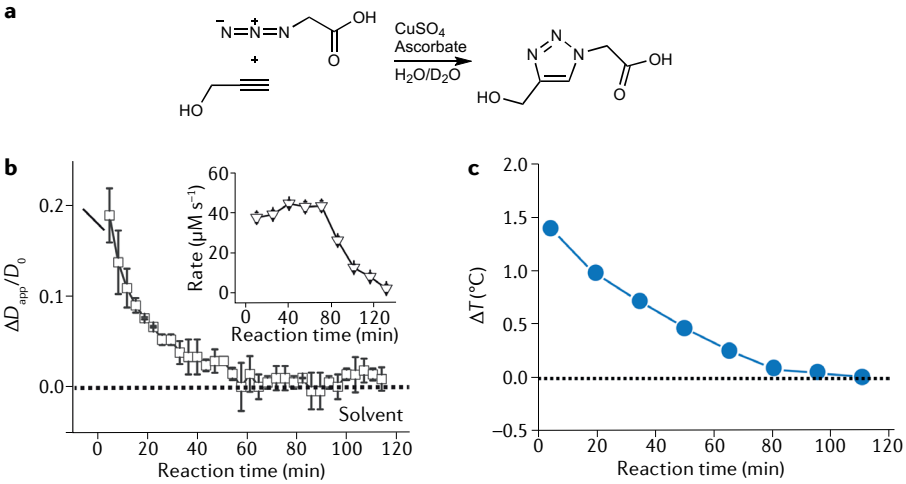

Fig. 4 | **Reported example of boosted molecular diffusion during azide–alkyne cycloaddition.** **a** | The Cu-catalysed reaction between propargyl alcohol and azidoacetic acid affords a triazole product. **b** | The apparent enhancement in diffusion ΔD_{app}, normalized with respect to the translational diffusion coefficient D_0, of H_2O/D_2O solvent decreases over the course of the reaction. Respective reaction rates are pictured in the inset. **c** | Change in temperature during the reaction follows a similar trend. Parts **b** and **c** adapted with permission from REF.[18], AAAS.

Einstein equation with a proper assessment of the effective radius of gyration of the diffusing entity in its environment[83]. The large ratio between drag and mass implies that any kinetic energy imparted on the swimmer during a reaction is quickly dissipated into heat through viscous friction, resulting in only a small displacement and negligible diffusion enhancement. For example, a 100-Da molecule with a radius of 1 nm and kinetic energy of $10\,k_BT$ travels only 6 pm in H_2O before the kinetic energy has dissipated into the environment. Boosts of kinetic energy of $10\,k_BT$ repeating at a frequency of $10^4\,s^{-1}$ would therefore increase the diffusion coefficient relative to the 'unboosted' molecule only by a fraction of 10^{-9}. Only by implicitly and inexplicably assuming a solution viscosity as low as that of air can nanometre-scale displacements be generated[21]. For this reason, observations of enhanced diffusion of small molecules such as Grubb's second-generation catalyst should come as a surprise[17] because they cannot be explained by the changes in molecular radii during the reaction nor the presence of a chemical gradient. This was followed by an equally puzzling finding that both the passive tracer molecules and the catalyst exhibited enhanced diffusion in a reaction-velocity-dependent manner[84]. These observations raise the fundamental questions of how the enhanced diffusion is powered by the catalytic reaction and how the energy and momentum are transferred from the reactive species to the environment[85]. Molecular dynamics simulations suggested that chemical reactions could cause a significant enhancement in diffusion coefficients for Ångström-scale catalysts in an 'argon-like solvent'[86], but the argon-like solvent has a viscosity that is more than 1,000-fold lower than the viscosity of H_2O or organic solvents. Of course, an increase in viscosity increases energy dissipation, decreases the displacement per catalytic event and decreases the diffusion enhancement. More generally, the study of intramolecular vibrational energy redistribution has shown that even if specific vibrational modes of a molecule are excited, the excitation spreads among the accessible vibrational modes on a femtosecond to picosecond timescale. This makes it difficult to channel the energy released from a reaction into a single degree of freedom, as would be necessary for propulsion[87,88].

The diffusion coefficient measurements of Grubbs' second-generation catalyst, first measured using diffusion NMR, have since been replicated at higher temporal resolution[89]. The apparent diffusion coefficient increased in the first 25 min and then fell back to normal, whereas the reaction rate decreased monotonically over time. No diffusion enhancement was found for reactions carried out in a narrow NMR tube. Collectively, these findings suggested that the observed enhanced diffusion of small molecules was caused by convection in the bulk solution.

The above discovery has not put an end to the debate regarding enhanced diffusion. Also using diffusion NMR, Wang et al. recently observed enhanced diffusion (by 2–20%) of reactants and catalysts, and even solvents, in common reactions including catalysed bimolecular reactions, azide–alkyne cycloaddition, ring-opening metathesis polymerization and Sonogashira coupling[18] (FIG. 4). By contrast, no enhancement was observed for S_N1 and S_N2 nucleophilic substitution reactions. Convection suppression pulses were applied to counteract reaction-induced convection. In parallel to the claims of enhanced enzyme diffusion during catalysis, it was claimed that the magnitude of diffusion enhancement was related to the free energy release rate. Shortly thereafter, another team showed that the apparent boost in mobility may originate from experimental artefacts caused by changes in signal intensities over time during the NMR measurements[90]. Such an effect could introduce systematic errors in the regression. When repeating the cycloaddition described by Wang et al., the team demonstrated that apparently faster or slower diffusion can be achieved simply by applying a monotonically increasing or decreasing magnetic field gradient. Wang et al. responded with experiments showing that the diffusion coefficients measured in randomized magnetic field gradients were identical to those measured in linearly changing gradients[91]. Furthermore, Wang et al. argued that the failure to reproduce the diffusion enhancement might be due to the different reaction rates.

Independent of the argument of whether boosted molecular diffusion is observable in diffusion NMR, there appear to be other inconsistencies in Wang et al.'s paper. For the click reaction, the diffusion coefficient of the solvent gradually decreased to a normal value within 60 min whereas the reaction rate was constant over almost 80 min (FIG. 4b). This suggests that the reaction caused enhanced diffusion in the beginning of the reaction, but not towards the end. It is unclear why this should be the case. Curiously, the time course of the change in the diffusion coefficient was similar to the time course of the change in the temperature, which started 1.5 K above room temperature and dropped to room temperature within 60 min (FIG. 4c). Temperature changes can affect the observed diffusion coefficient because they greatly affect the viscosity of the aqueous solvent and can create convection artefacts. In ring-opening metathesis polymerization with the Grubbs second-generation catalyst, the diffusion of species over the course of the reaction must also be substantially affected by changes in the composition and concentration of reactants that are present

at high initial concentrations (hundreds of mM to 1 M). However, this factor has not been quantitatively accounted for when the observed changes in diffusion coefficients are assigned wholly to enhanced diffusion. We look forward to seeing more detailed discussion of this intriguing but controversial report.

Enhanced transport of passive tracers

Tracer particles are traditionally used to visualize the flow field in fluid dynamics. Ideally, the tracer particles are inert and provide high contrast to facilitate observation, while being small and of sufficiently low molar mass to follow the path of the surrounding fluid. In the study of microswimmers, tracers can be smaller, of similar size or substantially larger than the microswimmers themselves. The tracers move not only because they interact with the microswimmers but also because of their own Brownian motion and other flow fields such as convection.

Tracer transport due to microswimmers. Microswimmers translate and rotate, exerting pressure and torque on surrounding fluid and establishing flow fields that could substantially affect the motion of passive tracer particles. The particles can be entrained forward if they are near the moving swimmer, and tend to move in closed loops if they are farther from the swimmer[92] (FIG. 5a). The tracer trajectories are governed by factors that include the geometry and size of the swimmer, the swimming path length and velocity, the distance between the swimmer and tracer, and boundary conditions. These can be further complicated by the Brownian motion of the tracer[93]. The increased mobility of tracers caused by active swimmers is of chemical and biological importance. For example, tracers in dilute suspensions of swimming bacteria exhibit enhanced diffusion[94]. Synthetic microswimmers have also shown an ability to agitate tracers. This enhanced diffusivity has been observed for 1–2 μm tracers in the presence of bimetallic Au–Pt rods (1.2 μm in length × 0.4 μm in diameter) swimming close to a surface through bipolar electrochemical propulsion[95,96]. The diffusion coefficient of the 2 μm tracer increased linearly from 0.15 to 0.3 $\mu m^2 s^{-1}$ as the swimmer density and velocity were increased. This observation fits well with a back-of-the-envelope calculation of the diffusion coefficient enhancement, which assumes that each tracer–swimmer encounter displaces the tracer by roughly the diameter of the swimmer. Tracer diffusion enhancement of 20–50% has also been measured in different enzymatic reactions for tracers ranging from the small-molecule rhodamine B to polystyrene particles of 50 nm and 100 nm, lending support to enzyme propulsion[97]. Puzzlingly, the tracer diffusion enhancement was the same for the fast enzyme urease and the 10^3× slower enzyme aldolase at the same enzyme concentration. This seems counterintuitive because the swimmer activity determines the frequency of encounters between swimmers and tracers, and thereby the tracer diffusion enhancement. Tracer motion in the presence of bubble-propelled micromotors was further amplified by the gravity-driven motion of the generated bubbles[98].

Reaction-induced convection. The concentration gradients produced by chemical reactions can give rise to convective flows that pump tracer particles (FIG. 5b). For example, surface-immobilized enzymes such as glucose oxidase, urease, lipase, catalase and DNA polymerase can pump fluids and particles in the presence of their substrates through convective flow[99,100]. The resulting flow velocity is on the order of micrometres per second and often increases with increasing reaction rates. Similarly, enzymatic reactions at the air–liquid interface of a homogeneous solution can also drive Rayleigh–Bénard-type convection if the reaction increases the solutal density, leading to flow velocities of up to 1 mm s^{-1} (REF.[101]). Because Rayleigh–Bénard-type convection occurs only above a critical

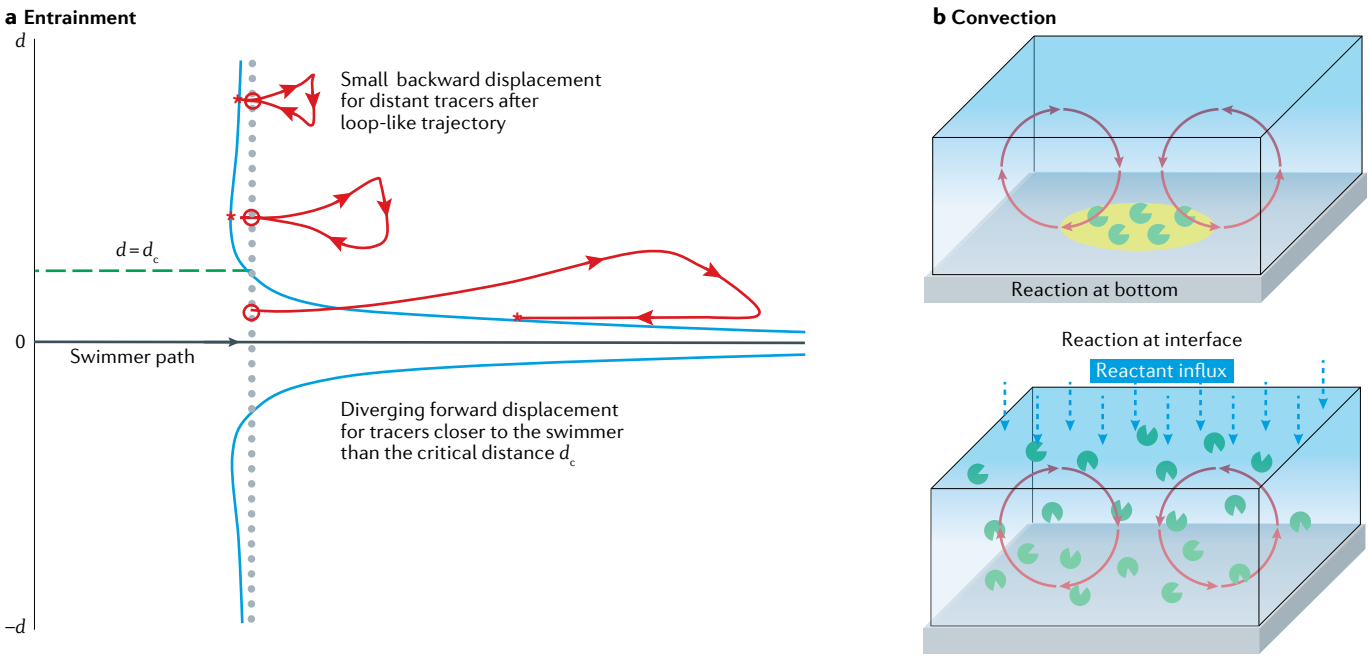

Fig. 5 | **Enhanced transport of tracers. a** | Typical trajectories of a sheet of tracer particles as a microswimmer moves from left to right. Initial positions of tracer particles shown as a grey dotted line and the envelope of their final positions in blue curves. Three trajectories of tracers (red curves) start from the open circles and end at the asterisks. Initial distance between the tracer and the swimmer path is denoted *d*. **b** | Tracer particles can be transported by convective flows induced by asymmetrically distributed reactions. These flows can be established by, for example, surfaces decorated with immobilized enzymes or the introduction of reactants such as O_2 at the interface of a fluid layer. Part **a** adapted with permission from REF.[92], Cambridge University Press.

barrier governed by the Rayleigh number (proportional to (solution depth)^3), the solution must typically be at least 1 mm deep. The contribution of thermal buoyancy in such systems is usually negligible[102] but the gradient in surface tension may play a more important role especially when the system dimensions become smaller[103]. The requirements for reaction-induced convection are frequently met in experiments aimed at finding enhanced diffusion, and convection has to be carefully ruled out as a mechanism responsible for the observations.

Reliability of diffusion measurements

Many papers report diffusion enhancements as small as 20%, such that the accuracy and precision of measurements is crucial. MSD analysis has been widely used as a standard measurement to determine diffusion coefficients of microswimmers[104], nanoswimmers[23] and even single enzymes[76]. A recent test on the reproducibility of MSD analysis has alerted the community to possible misinterpretations[77]. The test was conducted by tracing size-standard 100-nm spherical colloidal particles using a Nanosight NS300 (Malvern) instrument. Based on 244 particle tracks, the analysis afforded a precise and accurate diffusion coefficient, with errors smaller than 1%. However, using a subset of only 24 tracks can lead to results with 30% deviations. Although the errors should be non-directional, biased selection further widened the uncertainty from −55.5% to +68.0%. The experimental uncertainty also comes from the 2D projection of the 3D Brownian paths but can be lowered by increasing the size of the data set. The strikingly large inaccuracy indicated that MSD analysis with fewer than 50 tracks is unreliable for claiming a diffusion enhancement of 20% or less. Unfortunately, few investigations in the past decade used the desired sample size, rendering the measured enhancements potentially not statistically significant. A critical examination of the experimental error estimates is important when using these enhancements to claim statistical significance of observed enhanced diffusion. For example, estimates of experimental errors are likely too small if statistically significant variations in the diffusion enhancement are observed at different saturating substrate concentrations[76].

FCS can be applied to measure absolute diffusion coefficients of molecular and nanoscale swimmers by analysing fluctuations in emission from a few molecules freely diffusing in and out of the observation volume[105]. The standard deviation of autocorrelation functions has been studied analytically and experimentally[106–108] but the highly non-linear relationship between the diffusion coefficient and the autocorrelation function makes it hard to estimate the errors. A statistical analysis of diffusion coefficients extracted from FCS measurements suggested that their accuracy was sensitive to a molecule's brightness and concentration, as well as the measurement time[109]. To achieve a given accuracy, experimental conditions have to be carefully optimized otherwise FCS can be extremely error-prone. A satisfactory accuracy for the diffusion coefficient from FCS measurements is 10%[110] and according to a IUPAC Technical Report, dual-focus FCS — a more accurate modification of FCS — can further improve the accuracy to 4%[111]. However, FCS measurements are prone to artefacts caused by protein dissociation and aggregation, concentration changes due to surface adsorption, fluorophore quenching and the presence of freely diffusing dyes, often resulting in enhanced diffusion coefficients[74]. Granick and colleagues have defended the robustness of FCS, arguing that the influence of quenching is manageable if the timescales of diffusion can be well separated from the timescales of photophysical processes[112]. However, their experiments on dye-labelled bovine serum albumin still showed changes in the measured diffusion coefficient of ∼15% and >50% in the presence of 0.5 mM and 1 mM tryptophan (a fluorescence quencher), respectively, even though albumin does not catalyse any reactions[112]. In principle, stimulated emission depletion FCS facilitates diffusion measurements but in practice the method introduces new complexities, such as sensitivity to optical aberrations and potential interactions between the diffusing molecule and the high-power infrared laser[113,114].

In addition to the above methods targeting one or a few objects, DLS can assess the ensemble diffusivity of objects with sizes from several nanometres to micrometres. Most commercial DLS instruments are claimed to have a measurement accuracy of 2% according to International Standard ISO13321. Of course, this specification is achievable when using standard samples under optimized conditions. However, the R^6 dependence of scattering intensity makes the measurement extremely sensitive to particle aggregation and the presence of adventitious larger particles such as dust. Especially for proteins several nanometres in diameter, the weak scattering signal, the ease of aggregation, and the structural and thermal instability easily lower the accuracy. In practice, the uncalibrated viscosity of solutions containing different concentrations of reagents can also cause systematic inaccuracies of up to 5%. Variations in concentration, labware cleanliness and temperature will result in additional random uncertainties. It is common to expect an experimental error of at least 10% for protein samples unless special care has been taken during the measurement.

Diffusion NMR is a powerful technique to determine translational diffusion coefficients of molecules and can resolve different compounds with different diffusivities in a mixture according to their characteristic chemical shifts. The measurement makes use of NMR signal attenuation, which depends on both molecular diffusion and the applied magnetic field gradient pulses[115]. Although an accuracy of 2% is possible, achieving this demands high-quality data without spectral overlap and ideal experimental conditions[116]. Systematic artefacts mainly come from inherent non-uniformity of the field gradient based on the gradient coil design, convection triggered by temperature gradients and eddy currents caused by sudden gradient switching[116,117]. To achieve high-quality diffusion data, the gradient non-uniformity needs to be compensated for by pulse calibration[118], the convection needs to be avoided with a convection-compensated pulse sequence[115] and the eddy currents need to be reduced by using a shielded gradient system and/or a smoothly changing pulse[116]. If the experiments are not carefully carried out under optimized conditions, the measured diffusion coefficient can appear larger than it really is.

Overall, there exist various common techniques to measure diffusion, all of which have their associated errors. Given the typical accuracy and precision of these techniques, reported diffusion enhancements within 20% are on the edge of being statistically significant, especially for enzymes and synthetic swimmers at the nanoscale.

Applications and efficiencies of swimmers

The accelerated diffusion or locomotion of nanoswimmers and microswimmers, tracers and solvents has inspired applications in bioseparation, environmental remediation, detection, drug delivery and precision surgery, among others. Taking advantage

of the enhanced diffusion of enzymes in their corresponding substrate concentration gradient, chemotactic separation of active enzymes (catalase and urease) from inactive ones has been demonstrated in a microfluidic device[119], and anti-chemotactic migration of urease has also been proposed[54]. In addition, active swimmers can agitate the surrounding fluid, sense environmental changes, navigate living tissues and penetrate cell membranes[120]. In light of these properties, a series of creative and intriguing demonstrations have shown a broad range of applications, including the detection and decontamination of nerve agents[7,121], acid neutralization in vivo[122], biodetoxification of pathogenic bacteria and toxins[123] and intracellular delivery of small interfering RNA or drugs[8,124,125]. For example, self-propelled polymer–Pt composite micromotors can accelerate the oxidative detoxification of organophosphorus compounds[7], and enzyme-powered chemotactic polymersomes can cross the blood–brain barrier, an important property in neuromedicine[125]. These and other efforts have been discussed in detail in recent reviews[126–132].

Although the ability of some synthetic swimmers to harvest energy from their surroundings greatly broadens their possible applications, their energy conversion efficiency (the quotient of mechanical energy produced to chemical energy consumed) is far below that of biological counterparts (FIG. 6). For example, the motor protein kinesin catalyses exothermic ATP hydrolysis as it walks along a microtubule and can do mechanical work on an external load in excess of 50% of the chemical energy consumed[133]. More strikingly, the free energy transduction efficiency of the rotary motor F_1-ATPase has been reported to be nearly 100%[134], although the irreversible heat dissipation by torque-induced mechanical slip would lower it to 40–80%[135]. The bacterium *Escherichia coli*, a microscale natural swimmer that propels itself with rotating flagellar filaments, has an efficiency of 2%[136]. In comparison, synthetic swimmers are several orders of magnitude less efficient. For example, the energy conversion efficiency of Au–Pt nanorods (2 μm in length and 370 nm in diameter and swimming at a speed of 10 μm s^{-1}) propelled by the decomposition of H_2O_2 has been estimated to be 10^{-9} (REF.[29]), and the typical efficiency of self-electrophoretic bimetallic particles is on the order of 10^{-8}–10^{-9} (REF.[137]). After optimizing morphology and catalytic activity, the highest efficiency observed for a diffusiophoretic motor is 10^{-5} for a Ag-based Janus spherical particle[138]. Microswimmers propelled by bubble generation have so far exhibited an even lower efficiency of ~10^{-10}. It is possible to prepare helical nanobelts that mimic bacterial flagella and obtain an efficiency of 10^{-2}–10^{-3}, but the mimics are powered by an external rotating magnetic field rather than being self-propelled[29,139].

The extremely low efficiency of synthetic nanoswimmers and microswimmers (or motors) severely limits their application[140] because performing even small amounts of work requires enormous amounts of chemical fuel (for example, 1 M H_2O_2). This can cause toxicity and insolubility, but also leads to ambiguity — is the observed effect due to work or the vastly larger heat generated as a by-product by the motor? One of the mechanistic origins is a mismatch between the large forces that can be generated during the cleavage and formation of bonds and the small resistance offered by the fluid environment. Motor proteins are only efficient if they have a loaded cytoskeletal filament to pull against, and similarly the flagellar motor needs the flagellum as a transducer. In the examples discussed above, the catalytic particles 'swim' when they need to 'row' — they push locally against small loads, whereas a gearing mechanism such as an oar would enable a flow field with smaller velocity gradients (implying smaller frictional losses) and a better matching of force generation and load. Improving the efficiency will be crucial to develop the next generation of synthetic motors that can work in physiological environments with reasonable concentrations of potential fuels (such as glucose, O_2 and H^+). To realize a high-performance propulsion system, we require an efficient chemical–mechanical coupling mechanism as prime mover, a suitable power transmission system and a well-designed actuator to work in concert.

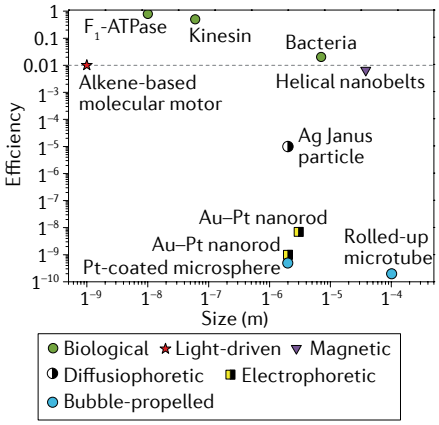

Fig. 6 | **Efficiencies of typical microscopic motors.** Kinesin[133], F_1-ATPase[135], *Escherichia coli*[136], alkene-based molecular motors[150], helical nanobelts[139], Ag Janus particles[138], Au–Pt nanorods[29,137], Pt-coated Janus particles[43] and rolled-up microtubes[151] have diverse propulsion mechanisms. Their efficiencies, several estimates of which were obtained from REF.[137], span several orders of magnitude. Note that the alkene-based molecular motor is driven by light irradiation and helical nanobelts are powered by external magnetic fields instead of chemical reactions.

Summary

Chemically-powered molecular and nanoswimmers/microswimmers that exhibit enhanced diffusion or swimming relative to the expected Brownian diffusion are desirable because they can convert chemical energy into potentially useful mechanical work. Molecular, nanoscale and microscale systems exhibiting diffusion enhancement have been intensively studied and hotly debated in the past decade. The debates have mainly focused on the underlying propulsion mechanisms and the size of the effect, which may vary from case to case as the swimmers differ in size and architectures. In this Perspective, we have systematically categorized reported observations of enhanced diffusion according to the sizes of the swimmers. Microscale (or larger) swimmers can exhibit ballistic motion whereas nanoscale or molecular-scale swimmers exhibit 'active' diffusion, with the observed diffusion enhancement typically being near the limits of experimental reproducibility and statistical significance. Rigorous analysis is thus desired to clarify the reliability, origin and achievable magnitude of diffusion enhancement.

The study of active diffusion on molecular scales, nanoscales and microscales opens an avenue to the design of synthetic machines that perform work in the presence of comparatively large thermal fluctuations. The implementation of these microscopic machines would enable us to steer chemical reactions and biological processes, and would consequently lead to revolutionary developments in diverse areas including, but not limited to, reaction regulation, cell manipulation and precision medicine. Although evolution has provided sophisticated examples such as motor proteins and transcriptional machineries, the construction of synthetic microscopic machines is challenging. The previously reported synthetic swimmers with enhanced diffusivity, regardless of their validation, are still much simpler and less efficient compared with their biological counterparts. Future efforts should focus on

understanding chemomechanical coupling and the structure–function relationship of these microscopic machines, so that we can gain fundamental insights for the construction of more sophisticated machines that may perform complex tasks beyond speeding up diffusion and mixing. For example, the latest advance in this field is a computational design of millimetre-size gears driven by enzymatic reaction-induced convections[141], putting us a step closer to constructing chemically-powered functional machines. We expect to see breakthroughs such as de-novo-designed protein motors and bioinorganic hybrid components and machines that can directly convert chemical energy into mechanical work. These efforts will greatly expand our toolbox on the molecular, subcellular and even macroscopic scales.

Yifei Zhang[1,2]✉ *and Henry Hess*[3]✉

[1]*Beijing Advanced Innovation Center for Soft Matter Science and Engineering, Beijing University of Chemical Technology, Beijing, China.*

[2]*State Key Laboratory of Chemical Resource Engineering, Beijing University of Chemical Technology, Beijing, China.*

[3]*Department of Biomedical Engineering, Columbia University, New York, NY, USA.*

✉*e-mail: yifeizhang@mail.buct.edu.cn; hhess@columbia.edu*

https://doi.org/10.1038/s41570-021-00281-6

Published online 27 May 2021

1. Lancia, F., Ryabchun, A. & Katsonis, N. Life-like motion driven by artificial molecular machines. *Nat. Rev. Chem.* **3**, 536–551 (2019).
2. Aprahamian, I. The future of molecular machines. *ACS Cent. Sci.* **6**, 347–358 (2020).
3. Wang, J. Can man-made nanomachines compete with nature biomotors? *ACS Nano* **3**, 4–9 (2009).
4. Ozin, G. A., Manners, I., Fournier-Bidoz, S. & Arsenault, A. Dream nanomachines. *Adv. Mater.* **17**, 3011–3018 (2005).
5. Carter, N. J. & Cross, R. A. Mechanics of the kinesin step. *Nature* **435**, 308–312 (2005).
6. García-López, V. et al. Molecular machines open cell membranes. *Nature* **548**, 567–572 (2017).
7. Orozco, J. et al. Micromotor-based high-yielding fast oxidative detoxification of chemical threats. *Angew. Chem. Int. Ed.* **52**, 13276–13279 (2013).
8. de Ávila, B. E.-F. et al. Micromotor-enabled active drug delivery for in vivo treatment of stomach infection. *Nat. Commun.* **8**, 272 (2017).
9. Saper, G. & Hess, H. Synthetic systems powered by biological molecular motors. *Chem. Rev.* **120**, 288–309 (2020).
10. Roke, D., Wezenberg, S. J. & Feringa, B. L. Molecular rotary motors: unidirectional motion around double bonds. *Proc. Natl Acad. Sci. USA* **115**, 9423–9431 (2018).
11. Zhang, L., Marcos, V. & Leigh, D. A. Molecular machines with bio-inspired mechanisms. *Proc. Natl Acad. Sci. USA* **115**, 9397–9404 (2018).
12. Noji, H., Yasuda, R., Yoshida, M. & Kinosita, K. Direct observation of the rotation of F_1-ATPase. *Nature* **386**, 299–302 (1997).
13. Soong, R. K. et al. Powering an inorganic nanodevice with a biomolecular motor. *Science* **290**, 1555–1558 (2000).
14. Dennis, J. R., Howard, J. & Vogel, V. Molecular shuttles: directed motion of microtubules along nanoscale kinesin tracks. *Nanotechnology* **10**, 232 (1999).
15. Hess, H. Toward devices powered by biomolecular motors. *Science* **312**, 860–861 (2006).
16. Magdanz, V. et al. Spermatozoa as functional components of robotic microswimmers. *Adv. Mater.* **29**, 1606301 (2017).
17. Pavlick, R. A., Dey, K. K., Sirjoosingh, A., Benesi, A. & Sen, A. A catalytically driven organometallic molecular motor. *Nanoscale* **5**, 1301–1304 (2013).
18. Wang, H. et al. Boosted molecular mobility during common chemical reactions. *Science* **369**, 537–541 (2020).
19. Muddana, H. S., Sengupta, S., Mallouk, T. E., Sen, A. & Butler, P. J. Substrate catalysis enhances single-enzyme diffusion. *J. Am. Chem. Soc.* **132**, 2110–2111 (2010).
20. Sengupta, S. et al. Enzyme molecules as nanomotors. *J. Am. Chem. Soc.* **135**, 1406–1414 (2013).
21. Riedel, C. et al. The heat released during catalytic turnover enhances the diffusion of an enzyme. *Nature* **517**, 227–230 (2015).
22. Ma, X., Hortelão, A. C., Patiño, T. & Sánchez, S. Enzyme catalysis to power micro/nanomachines. *ACS Nano* **10**, 9111–9122 (2016).
23. Ma, X. et al. Enzyme-powered hollow mesoporous Janus nanomotors. *Nano Lett.* **15**, 7043–7050 (2015).
24. Purcell, E. M. Life at low Reynolds number. *Am. J. Phys.* **45**, 3–11 (1977).
25. Ishimoto, K. & Yamada, M. A rigorous proof of the scallop theorem and a finite mass effect of a microswimmer. Preprint at https://arxiv.org/abs/1107.5938 (2011).
26. Lauga, E. Enhanced diffusion by reciprocal swimming. *Phys. Rev. Lett.* **106**, 178101 (2011).
27. Howse, J. R. et al. Self-motile colloidal particles: from directed propulsion to random walk. *Phys. Rev. Lett.* **99**, 048102 (2007).
28. Yamamoto, D. & Shioi, A. Self-propelled nano/micromotors with a chemical reaction: underlying physics and strategies of motion control. *KONA Powder Part J.* **32**, 2–22 (2015).
29. Paxton, W. F., Sen, A. & Mallouk, T. E. Motility of catalytic nanoparticles through self-generated forces. *Chem. Eur. J.* **11**, 6462–6470 (2005).
30. Lee, T. C. et al. Self-propelling nanomotors in the presence of strong Brownian forces. *Nano Lett.* **14**, 2407–2412 (2014).
31. Wang, W., Duan, W., Sen, A. & Mallouk, T. E. Catalytically powered dynamic assembly of rod-shaped nanomotors and passive tracer particles. *Proc. Natl Acad. Sci. USA* **110**, 17744–17749 (2013).
32. Bunea, A.-I., Pavel, I.-A., David, S. & Gáspár, S. Modification with hemeproteins increases the diffusive movement of nanorods in dilute hydrogen peroxide solutions. *Chem. Commun.* **49**, 8803–8805 (2013).
33. Jun, I.-K. & Hess, H. A biomimetic, self-pumping membrane. *Adv. Mater.* **22**, 4823–4825 (2010).
34. Abécassis, B., Cottin-Bizonne, C., Ybert, C., Ajdari, A. & Bocquet, L. Boosting migration of large particles by solute contrasts. *Nat. Mater.* **7**, 785–789 (2008).
35. Paustian, J. S. et al. Direct measurements of colloidal solvophoresis under imposed solvent and solute gradients. *Langmuir* **31**, 4402–4410 (2015).
36. Velegol, D., Garg, A., Guha, R., Kar, A. & Kumar, M. Origins of concentration gradients for diffusiophoresis. *Soft Matter* **12**, 4686–4703 (2016).
37. Golestanian, R., Liverpool, T. B. & Ajdari, A. Propulsion of a molecular machine by asymmetric distribution of reaction products. *Phys. Rev. Lett.* **94**, 220801 (2005).
38. Arqué, X. et al. Intrinsic enzymatic properties modulate the self-propulsion of micromotors. *Nat. Commun.* **10**, 2826 (2019).
39. Patiño, T. et al. Influence of enzyme quantity and distribution on the self-propulsion of non-Janus urease-powered micromotors. *J. Am. Chem. Soc.* **140**, 7896–7903 (2018).
40. Ismagilov, R. F., Schwartz, A., Bowden, N. & Whitesides, G. M. Autonomous movement and self-assembly. *Angew. Chem. Int. Ed.* **41**, 652–654 (2002).
41. Fournier-Bidoz, S., Arsenault, A. C., Manners, I. & Ozin, G. A. Synthetic self-propelled nanorotors. *Chem. Commun.* **4**, 441–443 (2005).
42. Sitt, A. et al. Microscale rockets and picoliter containers engineered from electrospun polymeric microtubes. *Small* **12**, 1432–1439 (2016).
43. Gibbs, J. G. & Zhao, Y.-P. Autonomously motile catalytic nanomotors by bubble propulsion. *Appl. Phys. Lett.* **94**, 163104 (2009).
44. Nourhani, A., Karshalev, E., Soto, F. & Wang, J. Multigear bubble propulsion of transient micromotors. *Research* **2020**, 7823615 (2020).
45. Wang, H., Zhao, G. & Pumera, M. Beyond platinum: bubble-propelled micromotors based on Ag and MnO_2 catalysts. *J. Am. Chem. Soc.* **136**, 2719–2722 (2014).
46. Gao, W., Pei, A. & Wang, J. Water-driven micromotors. *ACS Nano* **6**, 8432–8438 (2012).
47. Zhang, X., Chen, C., Wu, J. & Ju, H. Bubble-propelled jellyfish-like micromotors for DNA sensing. *ACS Appl. Mater. Interfaces* **11**, 13581–13588 (2019).
48. Abdelmohsen, L. K. E. A. et al. Dynamic loading and unloading of proteins in polymeric stomatocytes: formation of an enzyme-loaded supramolecular nanomotor. *ACS Nano* **10**, 2652–2660 (2016).
49. Nijemeisland, M., Abdelmohsen, L. K. E. A., Huck, W. T. S., Wilson, D. A. & van Hest, J. C. M. A compartmentalized out-of-equilibrium enzymatic reaction network for sustained autonomous movement. *ACS Cent. Sci.* **2**, 843–849 (2016).
50. Gao, W. et al. Artificial micromotors in the mouse's stomach: a step toward in vivo use of synthetic motors. *ACS Nano* **9**, 117–123 (2015).
51. Li, J. et al. Enteric micromotor can selectively position and spontaneously propel in the gastrointestinal tract. *ACS Nano* **10**, 9536–9542 (2016).
52. Wang, T., Zheng, M., Wang, L., Ji, L. & Wang, S. Crucial role of an aerophobic substrate in bubble-propelled nanomotor aggregation. *Nanotechnology* **31**, 355504 (2020).
53. Chi, Q., Wang, Z., Tian, F., You, J. & Xu, S. A review of fast bubble-driven micromotors powered by biocompatible fuel: low-concentration fuel, bioactive fluid and enzyme. *Micromachines* **9**, 537 (2018).
54. Jee, A.-Y., Dutta, S., Cho, Y.-K., Tlusty, T. & Granick, S. Enzyme leaps fuel antichemotaxis. *Proc. Natl Acad. Sci. USA* **115**, 14–18 (2018).
55. Zhao, X. et al. Substrate-driven chemotactic assembly in an enzyme cascade. *Nat. Chem.* **10**, 311–317 (2018).
56. Illien, P. et al. Exothermicity is not a necessary condition for enhanced diffusion of enzymes. *Nano Lett.* **17**, 4415–4420 (2017).
57. Golestanian, R. Synthetic mechanochemical molecular swimmer. *Phys. Rev. Lett.* **105**, 018103 (2010).
58. Golestanian, R. Enhanced diffusion of enzymes that catalyze exothermic reactions. *Phys. Rev. Lett.* **115**, 108102 (2015).
59. Tsekouras, K., Gabizon, R. C., Marqusee, R., Pressé, S., Bustamante, C. Comment on "enhanced diffusion of enzymes that catalyze exothermic reactions" by R. Golestanian. Preprint at https://arxiv.org/abs/1608.05433 (2016).
60. Golestanian, R. Reply to comment on "enhanced diffusion of enzymes that catalyze exothermic reactions". Preprint at https://arxiv.org/abs/1608.07469 (2016).
61. Illien, P., Adeleke-Larodo, T. & Golestanian, R. Diffusion of an enzyme: the role of fluctuation-induced hydrodynamic coupling. *EPL* **119**, 40002 (2017).
62. Adeleke-Larodo, T., Illien, P. & Golestanian, R. Fluctuation-induced hydrodynamic coupling in an asymmetric, anisotropic dumbbell. *Eur. Phys. J. E* **42**, 1–10 (2019).
63. Bai, X. & Wolynes, P. G. On the hydrodynamics of swimming enzymes. *J. Chem. Phys.* **143**, 165101 (2015).
64. Feng, M. & Gilson, M. K. A thermodynamic limit on the role of self-propulsion in enhanced enzyme diffusion. *Biophys. J.* **116**, 1898–1906 (2019).
65. Zhang, Y. & Hess, H. Enhanced diffusion of catalytically active enzymes. *ACS Cent. Sci.* **5**, 939–948 (2019).
66. Zhang, Y., Armstrong, M. J., Bassir Kazeruni, N. M. & Hess, H. Aldolase does not show enhanced diffusion in dynamic light scattering experiments. *Nano Lett.* **18**, 8025–8029 (2018).
67. Günther, J.-P., Majer, G. & Fischer, P. Absolute diffusion measurements of active enzyme solutions by NMR. *J. Chem. Phys.* **150**, 124201 (2019).
68. Chen, Z. et al. Single-molecule diffusometry reveals no catalysis-induced diffusion enhancement of alkaline phosphatase as proposed by FCS experiments. *Proc. Natl Acad. Sci. USA* **117**, 21328–21335 (2020).
69. Feng, M. & Gilson, M. K. Enhanced diffusion and chemotaxis of enzymes. *Annu. Rev. Biophys.* **49**, 87–105 (2020).
70. Jee, A.-Y., Tsvi, T. & Granick, S. Master curve of boosted diffusion for 10 catalytic enzymes. *Proc. Natl Acad. Sci. USA* **117**, 29435–29441 (2020).
71. Astumian, R. D. Microscopic reversibility as the organizing principle of molecular machines. *Nat. Nanotechnol.* **7**, 684–688 (2012).
72. Astumian, R. D. Thermodynamics and kinetics of molecular motors. *Biophys. J.* **98**, 2401–2409 (2010).
73. Astumian, R. D. Trajectory and cycle-based thermodynamics and kinetics of molecular machines: the importance of microscopic reversibility. *Acc. Chem. Res.* **51**, 2653–2661 (2018).

74. Günther, J.-P., Börsch, M. & Fischer, P. Diffusion measurements of swimming enzymes with fluorescence correlation spectroscopy. *Acc. Chem. Res.* **51**, 1911–1920 (2018).
75. Jee, A.-Y., Chen, K., Tlusty, T., Zhao, J. & Granick, S. Enhanced diffusion and oligomeric enzyme dissociation. *J. Am. Chem. Soc.* **141**, 20062–20068 (2019).
76. Xu, M., Ross, J. L., Valdez, L. & Sen, A. Direct single molecule imaging of enhanced enzyme diffusion. *Phys. Rev. Lett.* **123**, 128101 (2019).
77. Novotný, F. & Pumera, M. Nanomotor tracking experiments at the edge of reproducibility. *Sci. Rep.* **9**, 13222 (2019).
78. Seo, M., Park, S., Lee, D., Lee, H. & Kim, S. J. Continuous and spontaneous nanoparticle separation by diffusiophoresis. *Lab Chip* **20**, 4118–4127 (2020).
79. Schurr, J. M., Fujimoto, B. S., Huynh, L. & Chiu, D. T. A theory of macromolecular chemotaxis. *J. Phys. Chem. B* **117**, 7626–7652 (2013).
80. Agudo-Canalejo, J., Illien, P. & Golestanian, R. Phoresis and enhanced diffusion compete in enzyme chemotaxis. *Nano Lett.* **18**, 2711–2717 (2018).
81. Mohajerani, F., Zhao, X., Somasundar, A., Velegol, D. & Sen, A. A theory of enzyme chemotaxis: from experiments to modeling. *Biochemistry* **57**, 6256–6263 (2018).
82. Huang, R. et al. Direct observation of the full transition from ballistic to diffusive Brownian motion in a liquid. *Nat. Phys.* **7**, 576–580 (2011).
83. Rossi, C. & Bianchi, E. Diffusion of small molecules. *Nature* **189**, 822–824 (1961).
84. Dey, K. K. et al. Dynamic coupling at the Ångström scale. *Angew. Chem. Int. Ed.* **55**, 1113–1117 (2016).
85. Dey, K. K. Dynamic coupling at low Reynolds number. *Angew. Chem. Int. Ed.* **58**, 2208–2228 (2019).
86. Colberg, P. H. & Kapral, R. Ångström-scale chemically powered motors. *EPL* **106**, 30004 (2014).
87. Gruebele, M. & Wolynes, P. G. Vibrational energy flow and chemical reactions. *Acc. Chem. Res.* **37**, 261–267 (2004).
88. Hess, H., Asmis, K. R., Leisner, T. & Wöste, L. Vibrational wave packet dynamics in the silver tetramer probed by NeNePo femtosecond pump–probe spectroscopy. *Eur. Phys. J. D* **16**, 145–149 (2001).
89. MacDonald, T. S. C., Price, W. S., Astumian, R. D. & Beves, J. E. Enhanced diffusion of molecular catalysts is due to convection. *Angew. Chem. Int. Ed.* **58**, 18864–18867 (2019).
90. Günther, J.-P. et al. Comment on "boosted molecular mobility during common chemical reactions". *Science* **371**, eabe8322 (2021).
91. Wang, H. et al. Response to comment on "boosted molecular mobility during common chemical reactions". *Science* **371**, eabe8678 (2021).
92. Pushkin, D. O., Shum, H. & Yeomans, J. M. Fluid transport by individual microswimmers. *J. Fluid Mech.* **726**, 5–25 (2013).
93. Mathijssen, A. J. T. M., Pushkin, D. O. & Yeomans, J. M. Tracer trajectories and displacement due to a micro-swimmer near a surface. *J. Fluid Mech.* **773**, 498–519 (2015).
94. Morozov, A. & Marenduzzo, D. Enhanced diffusion of tracer particles in dilute bacterial suspensions. *Soft Matter* **10**, 2748–2758 (2014).
95. Miño, G. et al. Enhanced diffusion due to active swimmers at a solid surface. *Phys. Rev. Lett.* **106**, 048102 (2011).
96. Wang, Y. et al. Bipolar electrochemical mechanism for the propulsion of catalytic nanomotors in hydrogen peroxide solutions. *Langmuir* **22**, 10451–10456 (2006).
97. Zhao, X. et al. Enhanced diffusion of passive tracers in active enzyme solutions. *Nano Lett.* **17**, 4807–4812 (2017).
98. Orozco, J. et al. Bubble-propelled micromotors for enhanced transport of passive tracers. *Langmuir* **30**, 5082–5087 (2014).
99. Sengupta, S. et al. Self-powered enzyme micropumps. *Nat. Chem.* **6**, 415–422 (2014).
100. Sengupta, S. et al. DNA polymerase as a molecular motor and pump. *ACS Nano* **8**, 2410–2418 (2014).
101. Zhang, Y., Tsitkov, S. & Hess, H. Complex dynamics in a two-enzyme reaction network with substrate competition. *Nat. Catal.* **1**, 276–281 (2018).
102. Ortiz-Rivera, I., Shum, H., Agrawal, A., Sen, A. & Balazs, A. C. Convective flow reversal in self-powered enzyme micropumps. *Proc. Natl Acad. Sci. USA* **113**, 2585–2590 (2016).
103. Maroto, J. A., Pérez-Muñuzuri, V. & Romero-Cano, M. S. Introductory analysis of Benard–Marangoni convection. *Eur. J. Phys.* **28**, 311–320 (2007).
104. Cheang, U. K., Roy, D., Lee, J. H. & Kim, M. J. Fabrication and magnetic control of bacteria-inspired robotic microswimmers. *Appl. Phys. Lett.* **97**, 213704 (2010).
105. Elson, E. L. Fluorescence correlation spectroscopy: past, present, future. *Biophys. J.* **101**, 2855–2870 (2011).
106. Koppel, D. E. Statistical accuracy in fluorescence correlation spectroscopy. *Phys. Rev. A* **10**, 1938–1945 (1974).
107. Wohland, T., Rigler, R. & Vogel, H. The standard deviation in fluorescence correlation spectroscopy. *Biophys. J.* **80**, 2987–2999 (2001).
108. Saffarian, S. & Elson, E. L. Statistical analysis of fluorescence correlation spectroscopy: the standard deviation and bias. *Biophys. J.* **84**, 2030–2042 (2003).
109. Enderlein, J., Gregor, I., Patra, D. & Fitter, J. Statistical analysis of diffusion coefficient determination by fluorescence correlation spectroscopy. *J. Fluoresc.* **15**, 415–422 (2005).
110. Heinemann, F., Betaneli, V., Thomas, F. A. & Schwille, P. Quantifying lipid diffusion by fluorescence correlation spectroscopy: a critical treatise. *Langmuir* **28**, 13395–13404 (2012).
111. Enderlein, J. Fluorescence correlation spectroscopy (IUPAC Technical Report). *Pure Appl. Chem.* **85**, 999–1016 (2013).
112. Kandula, H. N., Jee, A.-Y. & Granick, S. Robustness of FCS (fluorescence correlation spectroscopy) with quenchers present. *J. Phys. Chem. A* **123**, 10184–10189 (2019).
113. Barbotin, A., Galiani, S., Urbančič, I., Eggeling, C. & Booth, M. J. Adaptive optics allows STED-FCS measurements in the cytoplasm of living cells. *Opt. Express* **27**, 23378–23395 (2019).
114. Tsuboi, Y., Shoji, T. & Kitamura, N. Optical trapping of amino acids in aqueous solutions. *J. Phys. Chem. C.* **114**, 5589–5593 (2010).
115. Pagès, G., Gilard, V., Martino, R. & Malet-Martino, M. Pulsed-field gradient nuclear magnetic resonance measurements (PFG NMR) for diffusion ordered spectroscopy (DOSY) mapping. *Analyst* **142**, 3771–3796 (2017).
116. Antalek, B. Using pulsed gradient spin echo NMR for chemical mixture analysis: how to obtain optimum results. *Concepts Magn. Reson.* **14**, 225–258 (2002).
117. Kiraly, P., Swan, I., Nilsson, M. & Morris, G. A. Improving accuracy in DOSY and diffusion measurements using triaxial field gradients. *J. Magn. Reson.* **270**, 24–30 (2016).
118. Connell, M. A. et al. Improving the accuracy of pulsed field gradient NMR diffusion experiments: correction for gradient non-uniformity. *J. Magn. Reson.* **198**, 121–131 (2009).
119. Dey, K. K. et al. Chemotactic separation of enzymes. *ACS Nano* **8**, 11941–11949 (2014).
120. Karshalev, E., Esteban-Fernández de Ávila, B. & Wang, J. Micromotors for "chemistry-on-the-fly". *J. Am. Chem. Soc.* **140**, 3810–3820 (2018).
121. Singh, V. V., Kaufmann, K., Esteban-Fernández de Ávila, B., Uygun, M. & Wang, J. Nanomotors responsive to nerve-agent vapor plumes. *Chem. Commun.* **52**, 3360–3363 (2016).
122. Li, J. et al. Micromotors spontaneously neutralize gastric acid for pH-responsive payload release. *Angew. Chem. Int. Ed.* **56**, 2156–2161 (2017).
123. Esteban-Fernández de Ávila, B. et al. Hybrid biomembrane-functionalized nanorobots for concurrent removal of pathogenic bacteria and toxins. *Sci. Robot.* **3**, eaat0485 (2018).
124. Esteban-Fernández de Ávila, B. et al. Acoustically propelled nanomotors for intracellular siRNA delivery. *ACS Nano* **10**, 4997–5005 (2016).
125. Joseph, A. et al. Chemotactic synthetic vesicles: design and applications in blood–brain barrier crossing. *Sci. Adv.* **3**, e1700362 (2017).
126. Jurado-Sánchez, B. & Wang, J. Micromotors for environmental applications: a review. *Environ. Sci. Nano.* **5**, 1530–1544 (2018).
127. Wang, J., Dong, R., Wu, H., Cai, Y. & Ren, B. A review on artificial micro/nanomotors for cancer-targeted delivery, diagnosis, and therapy. *Nano Micro Lett.* **12**, 11 (2019).
128. Ou, J. et al. Micro/nanomotors toward biomedical applications: the recent progress in biocompatibility. *Small* **16**, 1906184 (2020).
129. Peng, F., Tu, Y. & Wilson, D. A. Micro/nanomotors towards in vivo application: cell, tissue and biofluid. *Chem. Soc. Rev.* **46**, 5289–5310 (2017).
130. Katuri, J., Ma, X., Stanton, M. M. & Sánchez, S. Designing micro- and nanoswimmers for specific applications. *Acc. Chem. Res.* **50**, 2–11 (2017).
131. Li, J., Esteban-Fernández de Ávila, B., Gao, W., Zhang, L. & Wang, J. Micro/nanorobots for biomedicine: delivery, surgery, sensing, and detoxification. *Sci. Robot.* **2**, eaam6431 (2017).
132. Gao, C. Y. et al. Biomedical micro-/nanomotors: from overcoming biological barriers to in vivo imaging. *Adv. Mater.* **33**, 2000512 (2021).
133. Ramaiya, A., Roy, B., Bugiel, M. & Schäffer, E. Kinesin rotates unidirectionally and generates torque while walking on microtubules. *Proc. Natl Acad. Sci. USA* **114**, 10894–10899 (2017).
134. Kinosita, K., Yasuda, R., Noji, H. & Adachi, K. A rotary molecular motor that can work at near 100% efficiency. *Phil. Trans. R. Soc. B* **355**, 473–489 (2000).
135. Sumi, T. & Klumpp, S. Is F_1-ATPase a rotary motor with nearly 100% efficiency? Quantitative analysis of chemomechanical coupling and mechanical slip. *Nano Lett.* **19**, 3370–3378 (2019).
136. Chattopadhyay, S., Moldovan, R., Yeung, C. & Wu, X. L. Swimming efficiency of bacterium *Escherichia coli*. *Proc. Natl Acad. Sci. USA* **103**, 13712–13717 (2006).
137. Wang, W., Chiang, T.-Y., Velegol, D. & Mallouk, T. E. Understanding the efficiency of autonomous nano- and microscale motors. *J. Am. Chem. Soc.* **135**, 10557–10565 (2013).
138. Shah, Z. H. et al. Highly efficient chemically-driven micromotors with controlled snowman-like morphology. *Chem. Commun.* **56**, 15301–15304 (2020).
139. Zhang, L. et al. Characterizing the swimming properties of artificial bacterial flagella. *Nano Lett.* **9**, 3663–3667 (2009).
140. Armstrong, M. J. & Hess, H. The ecology of technology and nanomotors. *ACS Nano* **8**, 4070–4073 (2014).
141. Laskar, A., Shklyaev, O. E. & Balazs, A. C. Self-morphing, chemically driven gears and machines. *Matter* **4**, 600–617 (2021).
142. Dey, K. K. et al. Micromotors powered by enzyme catalysis. *Nano Lett.* **15**, 8311–8315 (2015).
143. Pavel, I.-A., Bunea, A.-I., David, S. & Gáspár, S. Nanorods with biocatalytically induced self-electrophoresis. *ChemCatChem* **6**, 866–872 (2014).
144. Wilson, D. A., Nolte, R. J. M. & van Hest, J. C. M. Autonomous movement of platinum-loaded stomatocytes. *Nat. Chem.* **4**, 268–274 (2012).
145. Paxton, W. F. et al. Catalytic nanomotors: autonomous movement of striped nanorods. *J. Am. Chem. Soc.* **126**, 13424–13431 (2004).
146. Ma, X., Wang, X., Hahn, K. & Sánchez, S. Motion control of urea-powered biocompatible hollow microcapsules. *ACS Nano* **10**, 3597–3605 (2016).
147. Kim, D., Liu, A., Diller, E. & Sitti, M. Chemotactic steering of bacteria propelled microbeads. *Biomed. Microdevices* **14**, 1009–1017 (2012).
148. Sattayasamitsathit, S., Kaufmann, K., Galarnyk, M., Vazquez-Duhalt, R. & Wang, J. Dual-enzyme natural motors incorporating decontamination and propulsion capabilities. *RSC Adv.* **4**, 27565–27570 (2014).
149. Mano, N. & Heller, A. Bioelectrochemical propulsion. *J. Am. Chem. Soc.* **127**, 11574–11575 (2005).
150. Cnossen, A., Kistemaker, J. C. M., Kojima, T. & Feringa, B. L. Structural dynamics of overcrowded alkene-based molecular motors during thermal isomerization. *J. Org. Chem.* **79**, 927–935 (2014).
151. Solovev, A. A., Mei, Y., Bermúdez Ureña, E., Huang, G. & Schmidt, O. G. Catalytic microtubular jet engines self-propelled by accumulated gas bubbles. *Small* **5**, 1688–1692 (2009).

Acknowledgements

Y.Z. acknowledges start-up funds from Beijing Advanced Innovation Center for Soft Matter Science and Engineering at Beijing University of Chemical Technology (BAIC202103). H.H. acknowledges financial support from National Science Foundation Division of Materials Research (NSF-DMR) grant 1807514.

Author contributions

All authors contributed equally to the preparation of the manuscript.

Competing interest

The authors declare no competing interests.

Publisher's note

Springer Nature remains neutral with regard to jurisdictional claims in published maps and institutional affiliations.

© Springer Nature Limited 2021